Structural and Electronic Properties of the Ru Pyrochlores $Bi_{2-y}Yb_yRu_2O_{7-\delta}$

Leqing Li and Brendan J. Kennedy*

School of Chemistry, The University of Sydney, Sydney, NSW 2006 Australia

Received June 17, 2003. Revised Manuscript Received August 3, 2003

The structures of 13 members in the series $Bi_{2-y}Yb_yRu_2O_{7-\delta}$ have been refined using high-resolution powder neutron diffraction data. The resulting structural parameters have been used to calculate the bandwidths for the oxides, and these show a smooth reduction in the t_{2g} bandwidth as the Yb content is increased. Resistivity measurements show a transition from metallic to semiconducting behavior occurs near $y \approx 0.9$. This corresponds to the point at which the oxygen vacancies are no longer present in the oxides. Evidence for disorder of the Bi cations is presented.

Introduction

Ruthenium pyrochlores of the type $A_2Ru_2O_{7-\delta}$ have been widely studied for many years because of both their potential technological importance and their unusual electronic properties.[1−13] When the A-type cation is a rare earth ion they are magnetic semiconductors, but metallic conductivity is observed when the A-type cation is an ion with a $6s^2$ outer shell configuration such as Tl^+, Pb^{2+}, or Bi^{3+}. The ruthenium 4d electrons are on the borderline between localized and itinerant behavior.

A common theme of a number of the studies of the ruthernate pyrochlores has been to probe the possible relationship between the oxygen vacancies in pyrochlores and their remarkable physical properties. The pyrochlore $A_2B_2O_6O'$ structure tolerates a high degree of vacancies on the O′ anion sites, so its composition is $A_2B_2O_6O_{7-\delta}$, if the distinction between O and O′ is not made. Beyerlein and co-workers[14] originally highlighted the structural importance of oxygen vacancies when they showed the presence of long-range oxygen-vacancy ordering in the pyrochlore $Pb_2Ru_2O_{6.5}$. Such oxygen-vacancy ordering has now been observed in a number of related pyrochlores.[15−17] More recently the correlation between the structure, oxygen stoichiometry, and electronic properties has been probed, as is well illustrated in the studies of Sleight and co-workers on the Tl−Ru−O pyrochlore.[6,10,18,19] Stoichiometric $Tl_2Ru_2O_{7.00}$, is cubic ($Fd\bar{3}m$) at room temperature and undergoes a first-order phase transition to an orthorhombic, *Pnma*, structure below 150 K. This is in contrast to the nonstoichiometric oxide, $Tl_2Ru_2O_{6.95}$, which is cubic down to 2 K. The physical properties of the ruthernates, most noticeably their electrical conductivity, also depend on the precise stoichiometry. It is not uncommon for pyrochlores with second and third row transition metals to exhibit a metal to nonmetal transition.[7,9,11,20] A further example of the variable physical properties of the pyrochlores comes from studies of $Bi_2Ru_2O_{7-\delta}$ by Carbonio and co-workers[21] who extended previous work by Facer et al.[8] and showed that it is possible to control the oxygen stoichiometry, and hence the structure and conductivity of $Bi_2Ru_2O_{7-\delta}$, by altering the annealing conditions.

Cox[7,22,23] investigated the differences between the metallic and semiconducting pyrochlores using $Bi_2Ru_2O_{7-\delta}$ and $Y_2Ru_2O_7$ as models. Cox concluded that the

* To whom correspondence should be addressed. Phone: 61-2-9351-2742. Fax: 61-2-9351-3329. E-mail: b.kennedy@chem.usyd.edu.au.

(1) Subramanian, M. A.; Aravamudan, G.; Subba Rao, G. V. *Prog. Solid State Chem.* **1983**, *15*, 55.
(2) Edgell, R. G.; Goodenough, J. B.; Hamnett, A.; Naish, C. C. *J. Chem. Soc., Faraday Trans.* **1983**, *I 79*, 893.
(3) Horowitz, H. S.; Longo, J. M.; Horowitz, H. H.; Lewandowski, J. T. *ACS Symp. Ser.* **1985**, *127*, 143.
(4) Felthouse, T. R.; Fraundorf, P. B.; Friedman, R. M.; Schosser, C. L. *J. Catal.* **1991**, *127*, 421.
(5) Garcia, P. F.; Ferreti, A.; Suna, A. *J. Appl. Phys.* **1982**, *53*, 5282.
(6) Jarrett, H. S.; Sleight, A. W.; Weiher, J. F.; Gulley, J. L.; Hoell, P. C. In *Valence Instabilities and Related Narrow Band Phenomena*; Parks, R. D., Ed.; Plenum Press: New York, 1977; p 545.
(7) Cox, P. A.; Goodenough, J. B.; Tavener, P. J.; Telles, D.; Edgell, R. G. *J. Solid State Chem.* **1986**, *62*, 360.
(8) Facer, G.; Elcombe, M. M.; Kennedy, B. J. *Aust. J. Chem.* **1993**, *46*, 1987.
(9) Kanno, R.; Takeda, Y.; Yamamoto, T.; Kawamoto, Y.; Yamamoto, O. *J. Solid State Chem.* **1993**, *102*, 106.
(10) Kanno, R.; Huang, J.; Sleight, A. W. In *Proceedings of the Fifth International Symposium on Advanced Nuclear Energy Research*; 1994; p 127.
(11) Kobayashi, H.; Kanno, R.; Kawamoto, Y.; Kamiyama, T.; Izumi, F.; Sleight, A. W. *J. Solid State Chem.* **1995**, *114*, 15.
(12) Kennedy, B. J.; Vogt, T. *J. Solid State Chem.* **1996**, *126*, 261.
(13) Field, M.; Kennedy, B. J.; Hunter, B. A. *J. Solid State Chem.* **2000**, ***151***, 25.
(14) Beyerlein, R. A.; Horowitz, H. S.; Longo, J. M.; Leonowicz, M. E.; Jorgensen, J. D.; Rotella, F. J. *J. Solid State Chem.* **1984**, *51*, 253.
(15) Alonso, J. A.; Cascales, C.; Rasines, I.; Pannetier, J. *Acta Crystallogr. Sect. C* **1989**, *45*, 3.
(16) Kennedy, B. J. *J. Solid State Chem.* **1996**, *123*, 14.
(17) Ismunandar; Kennedy, J.; Hunter, B. A. *J. Solid State Chem.* 1996, *130*, 81.
(18) Takeda, T.; Nagata, M.; Kobayashi, H.; Kanno, R.; Kawamoto, Y.; Takano, M.; Kamiyama, T.; Izumi, F.; Sleight, A. W. *J. Solid State Chem.* **1998**, *140*, 182.
(19) Takeda, T.; Kanno, R.; Kawamoto, Y.; Takano, M.; Sleight, A. W.; Hewat, A. W. *J. Matter Chem* **1999**, *9*, 215.
(20) Yamamoto, T.; Kanno, R.; Takeda, Y.; Yamamoto, O.; Kawamoto, Y.; Takano, M. *J. Solid State Chem.* **1994**, *109*, 372.
(21) Carbonio, R. E.; Alonso, J. A.; Martinez, J. L. *J. Phys. Condens. Matter* **1999**, *11*, 361.
(22) Cox, P. A.; Egdell, R. G.; Goodenough, J. B.; Hamnett, A.; Naish, C. C. *J. Phys. C.* **1983**, *16*, 6221.
(23) Cox, P. A. In *Transition Metal Oxides: An introduction to Their Electronic Structure and Properties*; Rowlinson, J. S., Halpern, J., Green, M. L. H., Mukaiyama, T., Eds.; Oxford University Press: New York, 1992; Vol. 27.

10.1021/cm034503q CCC: $25.00
Published on Web 09/06/2003

transition from metallic $Bi_2Ru_2O_{7-\delta}$ to semiconducting $Y_2Ru_2O_7$ is caused by narrowing of the conduction band, and suggested that 6s electrons in $Bi_2Ru_2O_{7-\delta}$ are relatively weakly bound and so form states above the oxygen 2p band in the energy. Interaction between the bismuth 6s and ruthenium 4d orbitals is anticipated to be a major factor in increasing the width of the conduction band. The observation of metallic conductivity in the perovskites $CaRuO_3$ and $SrRuO_3$, but not in the pyrochlore $Y_2Ru_2O_7$ demonstrates that structural factors are also important. Although both the perovskite and pyrochlore structures contain corner-sharing BO_6 octahedra, the Ru−O−Ru angle is smaller in the pyrochlore than in the perovskite and this weakens the indirect π overlap on which the conduction bandwidth depends.

Whangbo[24,25] explained the relationship between the crystal structure and conductivity of the ruthenium pyrochlores in terms of band theory using the Mott−Hubbard mechanism of electron localization. He developed a model that neglects interactions between the A_2O' and B_2O_6 layers, and using EHTM methods demonstrated that the bandwidths for metallic pyrochlores are wider than those for semiconducting pyrochlores.

Kanno, Yamamoto, and co-workers have reported extensive studies of the physical properties of ruthenium oxides of the type $Bi_{2-y}Ln_yRu_2O_7$ and $Pb_{2-y}Ln_yRu_2O_{7-\delta}$ where Ln is Y, La, or a lanthanide.[9,11,20] In general, Kanno and co-workers used X-ray diffraction methods to probe structural changes in those oxides at the M−NM transition, although it is expected that the strong X-ray scattering power of Pb, Bi, and the lanthanides will limit the precision of such structural studies. Nevertheless, their studies show the same trends in the evolution of the structural behavior at the M−NM transition as found by Kennedy and Vogt[12] in their more precise powder neutron diffraction studies of unsubstituted $A_2Ru_2O_{7-\delta}$ oxides where A = Pr, Nd, Tb, Yb[12] or in the substituted $Bi_{2-y}Nd_yRu_2O_{7-\delta}$ oxides.[13] Kennedy and Vogt concluded from structural studies of a number of ruthenium pyrochlores[12] of the type $A_2Ru_2O_{7-\delta}$ that when the Ru−O−Ru angle is larger than ∼133°, the Ru−O bond distance is sufficiently small, and $\delta > 0$, then the ruthenium pyrochlores will exhibit metallic conductivity.

Very recently Avdeev et al[26] reported that their structural refinements for bismuth ruthenate and its Co- and Cu-doped derivatives show evidence for static displacement of both Bi and O′ atoms from the ideal pyrochlore positions. This disorder is related to the stereochemical activity of the $6s^2$ electron pair of Bi^{3+}. Similar static disorder has been observed in other Bi^{3+},[27,28] Tl^+,[29] and Sn^{2+}[30,31] based pyrochlores. Avdeev[26] suggested such disorder is likely to be present in most pyrochlore compounds in which the A site is occupied by a cation having s^2 lone pair electrons.

To probe the relationship between conductivity and structure in ruthenium pyrochlores, the series $Bi_{2-y}Yb_yRu_2O_{7-\delta}$ (y = 0 to 1.375, 2.0) has been prepared, and the crystal and electronic structures have been analyzed using the powder neutron diffraction methods. In addition, the published structural information for the series $Bi_{2-y}Nd_yRu_2O_{7-\delta}$[13] has been used to calculate the t_{2g} bandwidth. These results are used to explain the metal versus semiconductor behavior in terms of the concept of Mott−Hubbard electron localization.[32]

Experimental Section

Synthesis. The samples $Bi_{2-y}Yb_yRu_2O_{7-\delta}$ (y = 0, 0.125, 0.250, 0.375, 0.500, 0.625, 0.750, 0.875, 1.000, 1.125, 1.250, 1.375, 2.000) were prepared by the solid-state reaction of stoichiometric quantities of Bi_2O_3 (Aldrich), Ru (Aithaca), and Yb_2O_3 (Aldrich). All materials were used as received. The appropriate stoichiometric amounts of Bi_2O_3, Yb_2O_3, and Ru powder were mixed with an acetone slurry and ground with a mortar and pestle until dry. Each mixture was transferred to an alumina crucible and placed in a muffle furnace at 650 °C for 24 h. The samples were then reground and returned to the same alumina crucible and reheated at 800 °C for approximately 72 h. This process of regrinding and reheating of the samples at increasing temperatures was continued to minimize the loss of the volatile ruthenium and bismuth oxides. The samples were heated for a further 24 h at 950 °C. The three samples with y = 0.125, 0.250, and 0.375 were finally heated at 1100 °C for 48 h. The remaining samples were reground and heated again at 1150 °C for 48 h and finally at 1200 °C for 48 h.

Instrumentation and Structure Refinement. The sample purity was confirmed by powder diffraction by using a Shimadzu S6000 diffractometer, operating with a Cu target at 40 kV, 30 mA. The divergence and scatter slits were set to 1° and the receiving slit was set to 0.30 mm. Data were collected in 0.01° steps over the range 10−110°. A trace amount of Yb_2O_3 was observed only in $Yb_2Ru_2O_7$ while the remaining $Bi_{2-y}Yb_yRu_2O_{7-\delta}$ (y = 0 to 1.375) compounds were single phase.

Room-temperature synchrotron X-ray diffraction patterns were recorded on the Debye−Scherrer diffractometer at beamline 20B, the Photon Factory, Japan.[33] The sample was finely ground and housed in a 0.3-mm capillary for the measurements. Data were collected over the angle range $5 \le 2\theta \le 125°$ using three image plates as the detector with an incident wavelength of λ = 0.782 Å.

The room-temperature neutron powder diffraction patterns were recorded over the range $0 < 2\theta < 155°$ in 0.05° steps using thermal neutrons of wavelength of 1.3710 Å on the HRPD at ANSTO.[34] The structures were refined using the Rietveld method implemented in the program RIETICA.[35] The background was defined by a fourth-order polynomial in 2θ and was refined simultaneously with the other profile and structural parameters during the structural refinements. A Voigt peak shape function was employed, where the Gaussian component has widths given by the function

$$\mathrm{FWHM}^2 = U \tan^2\theta + V \tan\theta + W$$

(24) Whangbo, M. H.; Lee, K. S. *J. Solid State Chem.* **1997**, *131*, 405.
(25) Whangbo, M. H.; Kennedy, B. J.; Koo, H. J. *J. Solid State Chem.* **1998**, *136*, 269.
(26) Avdeev, M.; Haas, M. K.; Jorgensen, J. D.; Cava, R. J. *J. Solid State Chem.* **2002**, *169*, 24.
(27) Radosavljevic, I.; Evans, J. S. O.; Sleight, A. W. *J. Solid State Chem.* **1998**, *136*, 63.
(28) Jones, R. H.; Knight, K. S. *J. Chem. Soc., Dalton Trans.* **1997**, *15*, 2551.
(29) Ganne, M.; Tournoux, M. *Mater. Res. Bull.* **1975**, *10*, 1313.
(30) Birchall, T.; Sleight, A. W. *J. Solid State Chem.* **1975**, 12.
(31) Cruz, L. P.; Savariault, J. M.; Rocha, J. *Acta Crystallogr. C* **2001**, *57*, 1001.
(32) Mott, N. F. *Metal−Insulator Transitions*; Barnes and Noble: New York, 1974.
(33) Sabine, T. M.; Kennedy, B. J.; Garrett, R. F.; Foran, G. J.; Cookson, D. J. *J. Appl. Crystallogr.* **1995**, *28*, 513.
(34) Howard, C. J.; Ball, C. J.; Davis, R. L.; Elcombe, M. M. *Aust. J. Phys.* **1983**, *36*, 507.
(35) Howard, C. J.; Hunter, B. A. *A Computer Program for Rietveld Analysis of X-ray and Neutron Powder Diffraction Patterns*; Lucas Heights Research Laboratories: NSW, Australia, 1998; pp 1−27.

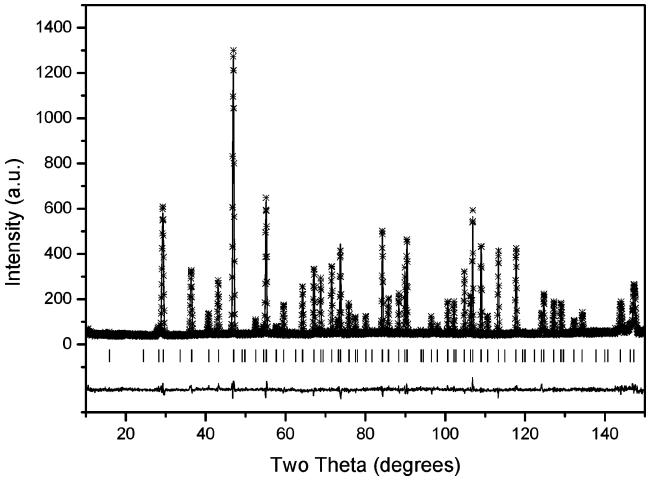

Figure 1. Observed, calculated, and difference neutron diffraction profiles for $Bi_{1.375}Yb_{0.625}Ru_2O_{7-\delta}$. The short vertical markers show the positions of all the allowed Bragg reflections ($\lambda = 1.372$ Å).

Table 1. Exponents ζ_i and Valence Shell Ionization Potentials H_{ii} of Slater-Type Orbitals χ_i Used for Extended-Huckel Tight-Binding Calculations[a]

atom	χ_i	H_{ii}	ζ_i	c_1[b]	ζ_i'	c_2[b]
Ru	5s	−6.43	2.091	1.000		
Ru	5p	−3.49	1.420	1.000		
Ru	4d	−15.3	4.357	0.5394	2.256	0.6062
O	2s	−33.7	2.246	1.000		
O	2p	−17.1	2.227	1.000		

[a] H_{ii}s are the diagonal matrix elements $\langle\chi_i/H^{eff}/\chi_i\rangle$, where H^{eff} is the effective Hamiltonian. In our calculations of the off-diagonal matrix elements $H^{eff} = \langle\chi_i/H^{eff}/\chi_i\rangle$, the weighted formula was used; see ref 2. [b] Contraction coefficients used in the double-ζ Slater-type orbital.

with refinable parameters *U*, *V*, and *W*. The width of the Lorentzian component was varied as η sec θ to model particle size effects and a peak asymmetry parameter was included. Anisotropic displacement parameters have been refined. The following constraints were applied in keeping with the site symmetry. For the 16c (Bi or Yb atoms) and 16d (Ru atoms), $\beta_{11} = \beta_{22} = \beta_{33}$ and $\beta_{12} = \beta_{13} = \beta_{23}$; for the 48f site (O atoms), $\beta_{22} = \beta_{33}$ and $\beta_{12} = \beta_{13} = 0$; and for the 8b site (O′ atoms), $\beta_{11} = \beta_{22} = \beta_{33}$, $\beta_{12} = \beta_{13} = \beta_{23} = 0$. The O′ site occupancies were also refined. A typical fit is shown in Figure 1.

The electrical resistivity was measured with sintered disks with dimensions of approximately 13 × 2 mm. The conductivity was measured by an AC four-probe method in the temperature range 4 K ≤ *T* ≤ 300 K using a Quantum Design physical property system. A helium cryostat with a temperature range from 4 to 310 K was used in the conductivity measurements. The temperature was monitored with a calibrated carbon-glass thermometer mounted near the sample.

Electronic Band Structures. The primary purpose of the extended-Hückel tight-binding (EHTB) calculations is to find the widths of the partially filled Ru d-bands. The energy band of the ruthenium pyrochlores is easily constructed assuming strong bonding within the Ru_2O_6 and A_2O' networks.[1] The simplest model to construct is provided by a binary chain,[36] composed alternately of Ru and O atoms. For the ruthenium pyrochlore, the most important valence orbitals are the p shell

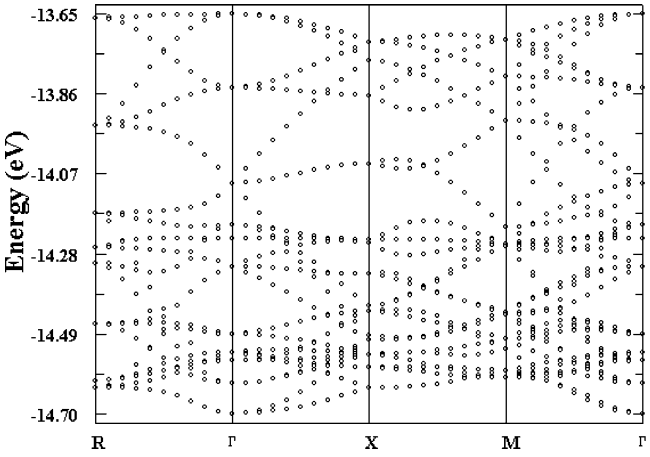

Figure 2. Band structure for $Bi_2Ru_2O_{7-\delta}$.

on the more electronegative O atom, and the d orbitals (d_{xy}, d_{yz}, d_{xz}, $d_{x^2-y^2}$, d_{z^2}) of the less electronegative Ru atom. To start with, it is supposed that these are the only atomic orbitals: that is, Ru has valence d orbitals, and O has one valence p orbital, pointed along the chain so as to overlap with the Ru d orbitals. The unit cell of the lattice now has two atoms, and two atomic orbitals. Although the actual unit cell is more complicated, the wave functions can be described by Bloch functions. Thus, the crystal orbitals can be written as Bloch sums of atomic orbitals, where each sum has a contribution from both of the atoms in the unit cell. Because there are two atomic orbitals, there will be two crystal orbitals for each *k* value, corresponding to bonding and antibonding combinations.

If the atomic orbitals on Ru and O at position *n* in the chain are written $\chi(\mathrm{Ru})_n$ and $\chi(\mathrm{O})_n$, the bonding and antibonding crystal orbitals can be written as

$$\Psi_k = \sum_{N=1}^{N} \exp(ikna)[a_k x(\mathrm{Ru})_n + b_k x(\mathrm{O})_n]$$

and

$$\Psi'_k = \sum_{N=1}^{N} \exp(ikna)[a_k x(\mathrm{Ru})_n - b_k x(\mathrm{O})_n]$$

where a_k and b_k are mixing coefficients, which depend on the energies and the degree of overlap between the Ru and O orbitals. The mixing also depends on the wavenumber *k*. In the present ruthenium pyrochlores, it is expected that when observed, metallic character will come from the width of the Ru 4d bands. However, the ruthenium atoms in the pyrochlore are too far apart for effective direct overlap of the Ru d orbitals. Consequently the main contribution to the bandwidth must be from indirect covalent interactions of the ruthenium 4d and O 2p orbitals. Covalent bonding is enhanced by the high formal oxidation state of ruthenium, which draws the 5d orbitals down in energy, closer to that of the oxygen orbitals.

In the EHTB calculation, only the Ru_2O_6 sublattice was considered (i.e., the A_2O sublattice was neglected). The program Caesar[37] has been used throughout. The atomic parameters used in the EHTB calculation are listed in Table 1.

A typical example of EHTB calculation using Caesar is given in Figure 2, which is similar to that previously reported by Whangbo using the same method.[24] This figure shows the dispersion relations of the t_{2g}-block bands calculated for $Bi_2Ru_2O_7$, where the lowest and highest points of the t_{2g} band calculated at the Γ point determine the overall width of the t_{2g} bands. This is also the case for the other ruthenium pyrochlores.

Result and Discussion

Synthesis. Single-phase samples of the substituted pyrochlores $Bi_{2-y}Yb_yRu_2O_{7-\delta}$ were obtained using stan-

(36) Cox, P. A. *The Electronic Structure and Chemistry of Solids*; Oxford University Press: New York, 1987; p 88.
(37) Ren, J.; Liang, W.; Whangbo, M.-H. *Caesar 1.0. PrimeColor Software*; SAS Inc.: Cary, NC, 1998.
(38) Sleight, A. W. *Inorg. Chem.* **1965**, *7*, 1704.
(39) Facer, G. R.; Howard, C. J.; Kennedy, B. J. *Powder Diffr.* **1993**, 8.
(40) Kennedy, B. J. *Physica B* **1998**, *241−243*, 302.

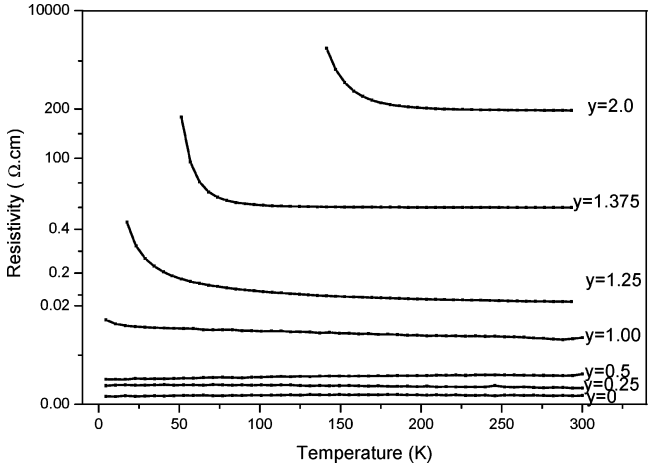

Figure 3. Temperature dependence of the resisitivity for selected members of the series $Bi_{2-y}Yb_yRu_2O_{7-\delta}$.

dard solid-state methods. For the $y = 0$ to 1.375 range of solid solutions, the firing temperature required to produce a single-phase material increased from 950 to 1200 °C with increasing ytterbium content. For $y =$ 1.500 to 2.000, trace amounts of Yb_2O_3 were observed in all samples, although the amount of Yb_2O_3 in the samples could be minimized by pressing the samples into 13-mm-diameter disks and heating at 1200 °C. It was not possible to obtain samples with $y \geq 1.5$ totally free of Yb_2O_3.

Electrical Properties. Electrical resistivity data for various $Bi_{2-y}Yb_yRu_2O_7$ oxides are shown in Figure 3. The data show that $Bi_2Ru_2O_7$ is metallic with a low and nearly temperature-independent resistivity of $\rho = 4 \times 10^{-3}$ Ω·cm, whereas in $Yb_2Ru_2O_7$, semiconducting properties were observed with a room-temperature resistivity of $\rho = 2 \times 10^2$ Ω·cm. Comparing to data given by Yamamoto and Kanno,[9,20] the resistivity observed here for $Bi_2Ru_2O_{7-\delta}$ is approximately the same ($\approx 5 \times 10^{-3}$ Ω·cm) at room temperature. As illustrated by Figure 3 the resistivity increases with increasing Yb content and a change from metallic to semiconducting behavior is observed between $y = 0.500$ and 1.000.

Powder Diffraction Results. To obtain accurate structural information, powder neutron diffraction data were collected for the series of $Bi_{2-y}Yb_yRu_2O_{7-\delta}$ pyrochlores. The strategy used was as follows. First, the lattice parameters of the oxides were determined using a conventional (Cu Kα) powder diffractometer, where tungsten ($a = 3.6150$ Å) was added as an internal standard. Next, a second X-ray diffraction data set was collected for each sample using identical conditions and this was jointly analyzed with the appropriate powder neutron diffraction data. In the joint analysis the lattice parameters for the various solid solutions were constrained to the value obtained from the analysis of the X-ray diffraction pattern for the W-containing sample, and the neutron diffractometer zero point and neutron wavelength were allowed to vary in the Rietveld refinements. A typical example of neutron diffraction refinement is given Figure 1. The selected bond distances, bond angles, and bond-valence from the refined structures are listed in Table 2.

In the structural refinements, anisotropic displacement parameters were employed and the O′ occupancies were also refined. In keeping with the previous studies of Sleight[38] and Facer et al,[39] we have found that in the ruthenium pyrochlores the displacement of the A-type, Bi(Yb), atoms is both large and highly anisotropic. For the Ru atoms, the thermal motion is much smaller as a consequence of the more regular coordination sphere around the Ru atom and the displacement is essentially isotropic. The displacements of the two types of oxygen atoms are noticeably different. The O′ atom has four nearest Bi(Yb) neighbors in tetrahedral arrangement and vibrates essentially isotropically. The second type of oxygen atom has C_{2v} site symmetry with two nearest Ru atoms and two more distant Bi(Yb) neighbors, and the displacement is highly anisotropic. These are illustrated in Figure 4.

The refined displacement parameters for the O′ atoms on the 8b sites are unusually large. In general, large displacement parameters can arise if there is (i) enhancement by a corresponding soft mode associated with a structure phase transition; (ii) static disorder of the atoms about the crystal; or (iii) nonstoichiometry on the appropriate site. Variable temperature measurements, to be described in a subsequent paper, showed the sample remains cubic to 10 K suggesting this is not a consequence of a soft mode. Refinements including anion vacancies resulted in better fit to the observed data, demonstrating this suggestion to be appropriate. The amount of these vacancies tended to increase as the Bi content increased, as is illustrated in Figure 5. Samples with $y > 0.750$ appear to have a near fully occupied 8b site. Samples with $y \leq 0.75$ have a significant number of vacancies at the O′ site. As described in more detail below, these samples ($y = 0$, 0.125, 0.250, 0.375, 0.500) are the metallic oxides. This phenomenon is similar to that observed by Field et al in the series $Bi_{2-y}Nd_yRu_2O_{7-\delta}$.[13]

Table 2. Refined Structural Parameters for $Bi_{2-y}Yb_yRu_2O_{7-\delta}$ at Room Temperature[a]

composition	a (Å)	x (O)	B(Bi/Yb)	B(Ru)	B (O1)	B(O2)	δ	Ru−O(1)	Bi−O(1)	Bi−O(2)	R_p	R_{wp}	GOF
$Bi_2Ru_2O_7$	10.2922(1)	0.3263(1)	1.76(3)	0.36(2)	0.71(1)	1.64(8)	0.048(1)	1.9815(4)	2.5509(7)	2.2282(3)	5.45	6.86	1.88
$Bi_{1.875}Yb_{0.125}Ru_2O_7$	10.2846(2)	0.3271(1)	1.51(2)	0.34(2)	0.73(1)	1.18(8)	0.079(1)	1.9834(4)	2.5423(7)	2.2259(3)	5.58	6.76	1.76
$Bi_{1.750}Yb_{0.250}Ru_2O_7$	10.2711(1)	0.3278(1)	1.38(2)	0.34(2)	0.76(1)	1.02(7)	0.045(1)	1.9837(4)	2.5345(7)	2.2236(3)	5.39	6.64	1.80
$Bi_{1.625}Yb_{0.375}Ru_2O_7$	10.2599(2)	0.3284(2)	1.35(3)	0.41(2)	0.87(2)	0.90(8)	0.046(1)	1.9839(5)	2.5379(9)	2.2212(3)	6.07	7.61	1.72
$Bi_{1.500}Yb_{0.500}Ru_2O_7$	10.2478(2)	0.3290(2)	1.20(3)	0.48(3)	0.90(2)	0.8(1)	0.030(1)	1.9844(7)	2.5203(9)	2.2188(4)	5.66	6.70	1.60
$Bi_{1.375}Yb_{0.625}Ru_2O_7$	10.2366(2)	0.3298(2)	1.17(3)	0.48(3)	0.97(2)	0.7(1)	0.042(1)	1.9853(7)	2.512(1)	2.2162(4)	5.51	6.55	1.57
$Bi_{1.250}Yb_{0.750}Ru_2O_7$	10.2258(2)	0.3302(2)	1.14(3)	0.62(3)	1.01(2)	0.6(1)	0.033(1)	1.9853(7)	2.506(1)	2.2136(5)	5.88	7.03	1.66
$Bi_{1.125}Yb_{0.875}Ru_2O_7$	10.2120(2)	0.3311(2)	1.05(3)	0.50(3)	0.89(2)	0.68(9)	0.004(1)	1.9862(5)	2.496(1)	2.2105(4)	6.31	7.70	1.77
$Bi_{1.000}Yb_{1.000}Ru_2O_7$	10.1958(2)	0.3318(2)	0.98(3)	0.61(3)	0.94(2)	0.7(1)	0	1.9858(7)	2.498(1)	2.2073(5)	6.59	8.01	1.82
$Bi_{0.875}Yb_{1.125}Ru_2O_7$	10.1808(2)	0.3325(1)	0.77(2)	0.39(2)	0.76(2)	0.56(7)	0	1.9861(5)	2.4800(8)	2.2047(4)	5.22	6.44	1.61
$Bi_{0.750}Yb_{1.250}Ru_2O_7$	10.1576(2)	0.3333(1)	0.68(2)	0.42(2)	0.75(2)	0.61(6)	0	1.9850(5)	2.4683(7)	2.1994(3)	5.06	6.27	1.61
$Bi_{0.625}Yb_{1.375}Ru_2O_7$	10.1405(2)	0.3343(1)	0.63(2)	0.44(2)	0.71(2)	0.69(7)	0	1.9859(5)	2.4576(8)	2.1959(4)	4.74	5.83	1.49

[a] The atoms are at the following positions in space group $Fd3m$ (No. 227): Bi onto a 16d ($^1/_2$, $^1/_2$, $^1/_2$), Ru 16c (0, 0, 0), O(1) 48f (x, $^1/_8$, $^1/_8$), and O(2) 8b (0.375, 0.375, 0.375).

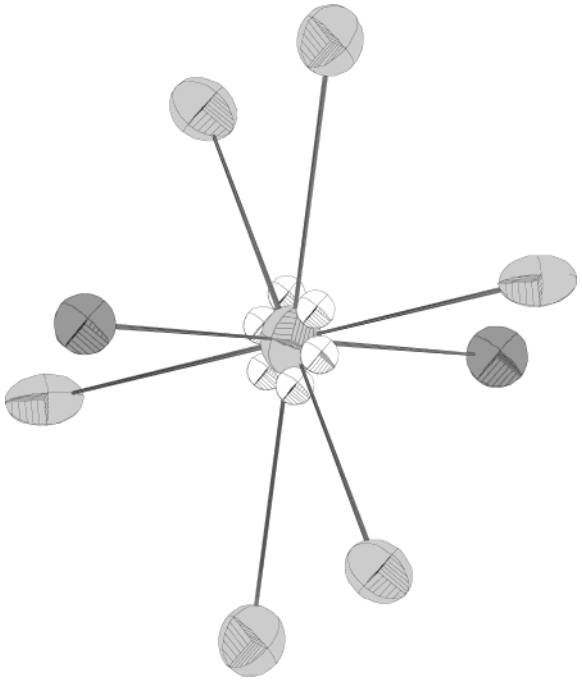

Figure 4. Local geometry of the Bi atoms in the pyrochlore structure. The central Bi atom is represented both as a pancake at the ($^1/_2$, $^1/_2$, $^1/_2$) position and as disordered over the corresponding 96h sites. The ellipsoids for the two different O atoms illustrate the approximate spherical displacement of the oxygen atoms on the 8b site and elongated displacement of those on the 48f site.

Although the final structural refinements used anisotropic displacement parameters, the variation of the equivalent isotropic values is informative. The equivalent isotropic displacement parameters for Bi and O′ show a systematic reduction as the Yb content increases, whereas those for Ru and O are essentially independent of Yb content (Table 2). At the same time the effective bond valence for the Bi/Yb cations is somewhat higher than expected (Table 3).

The Bi/Yb atoms have 8-fold coordination geometry where the oxygen atoms are located at the corners of a compressed scalenohedron. The Bi atoms have two principle vibrations given by $U_{11} + 2U_{12}$ parallel to the (1 1 1) direction and $U_{11} - U_{12}$ perpendicular to this. In all cases movements of the Bi along the 3-fold axis, that is toward the closest oxygen atom is, as expected, strongly inhibited. This is illustrated in Figure 4. The refinements suggested that there was little nuclear density near the center of the ($^1/_2$, $^1/_2$, $^1/_2$) position and a structural model in which the Bi was displaced onto a nearby 96h site at (0.5, $^1/_2 + y$, $^1/_2 - y$), $y \approx 0.25$ was investigated. Although this model did not result in any improvement in the various measures of fit for all compounds, Table 4, it did significantly lower the isotropic displacement parameter for the Bi atoms. Clearly X-ray diffraction data are expected to be more sensitive to cation disorder and we sought to confirm the nature of the Bi displacement using synchrotron XRD methods. As shown in Figure 6 the fit to the synchrotron data with a model in which Bi disorder is included significantly improves the quality of the fit. These results are entirely consistent with the very recent work of Avdeev.[26] Equally importantly, the displacement parameters for the Bi showed a systematic decrease with the largest decrease occurring for the Bi−Rich oxides; for example, B_{iso}(Bi) in $Bi_2Ru_2O_{6.9}$, decreases from 1.76 Å^2 to 1.00 Å^2, Table 5. In principle, displacement of the Bi atoms in the (0 $\bar{1}$ 1) direction will reduce a corresponding Bi−O bond distance and might be expected to cause displacement of the neigh-

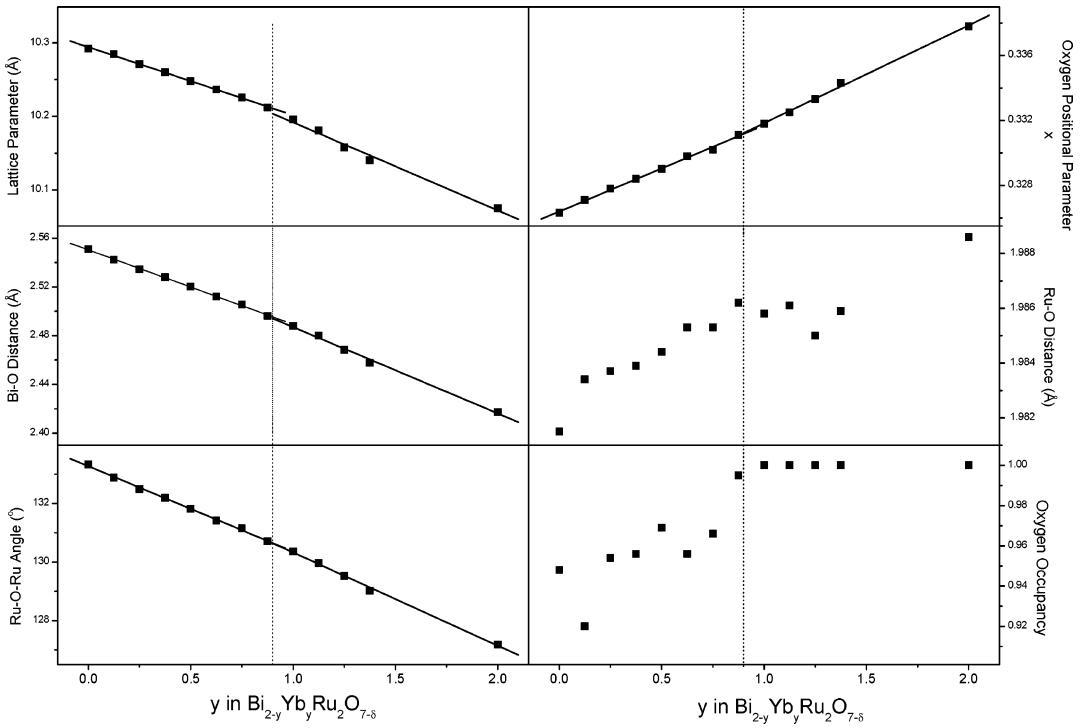

Figure 5. Composition dependence of selected structural features in the series $Bi_{2-y}Yb_yRu_2O_{7-\delta}$. In all cases the approximate position of the metal-semiconductor transition is indicated by the dashed line. The solid lines represent linear fits to the data above and below the critical compositions. For both the lattice parameters and Bi−O distances a clear break is observed near $y \approx 0.9$, whereas for the Ru−O−Ru angle and the oxygen positional parameter, y, the discontinuity is much less obvious.

Table 3. Selected Bond Angles and Bond Valence Sums for $Bi_{2-y}Yb_yRu_2O_{7-\delta}$ at Room Temperature[a]

				ordered Bi		disordered Bi	
composition	Ru−O−Ru	O(1)−Ru−O(1)	O(2)−Ru−O(2)	Ru BVS	Bi BVS	Ru BVS	Bi BVS
$Bi_2Ru_2O_7$	133.33(5)	95.34(4)	84.67(4)	4.03	3.11	4.03	3.17
$Bi_{1.875}Yb_{0.125}Ru_2O_7$	132.89(6)	95.63(4)	84.37(4)	4.01	3.09	4.01	3.15
$Bi_{1.750}Yb_{0.250}Ru_2O_7$	132.49(5)	95.89(4)	84.11(4)	4.00	3.09	4.00	3.14
$Bi_{1.625}Yb_{0.375}Ru_2O_7$	132.19(7)	96.09(5)	83.91(5)	4.00	3.09	4.00	3.13
$Bi_{1.500}Yb_{0.500}Ru_2O_7$	131.82(8)	96.33(6)	83.67(6)	4.00	3.09	4.00	3.12
$Bi_{1.375}Yb_{0.625}Ru_2O_7$	131.42(9)	96.60(6)	83.40(6)	3.99	3.08	3.99	3.12
$Bi_{1.250}Yb_{0.750}Ru_2O_7$	131.15(10)	96.77(6)	83.23(6)	3.99	3.07	3.99	3.10
$Bi_{1.125}Yb_{0.875}Ru_2O_7$	130.71(8)	97.06(5)	82.94(5)	3.98	3.07	3.98	3.09
$Bi_{1.000}Yb_{1.000}Ru_2O_7$	130.36(9)	97.30(6)	82.70(6)	3.98	3.08	3.98	3.09
$Bi_{0.875}Yb_{1.125}Ru_2O_7$	129.97(6)	97.54(4)	82.46(4)	3.97	3.06	3.98	3.10
$Bi_{0.750}Yb_{1.250}Ru_2O_7$	129.53(6)	97.83(4)	82.17(4)	3.99	3.09	3.99	3.10
$Bi_{0.625}Yb_{1.375}Ru_2O_7$	129.02(6)	98.16(4)	81.84(4)	3.98	3.09	3.98	3.11

[a] Bond valence sums have been calculated for both the ordered and disordered models.

Table 4. Refined Structural Parameters for $Bi_{2-y}Yb_yRu_2O_{7-\delta}$ at Room Temperature Allowing for Disorder of the Bi onto the 96h Site[a]

composition	*y* (Bi)	*x* (O)	B(Bi/Yb)	B(O)	δ	Ru−O(1)	Bi−O(1)	Bi−O(2)	R_p	R_{wp}	GOF
$Bi_2Ru_2O_7$	0.2390(4)	0.3263(1)	0.98(6)	1.37(17)	0.051(1)	1.9815(4)	2.556(4) 2.689(1) 2.416(1)	2.234(4)	5.47	6.88	1.88
$Bi_{1.875}Yb_{0.125}Ru_2O_7$	0.2388(4)	0.3271(1)	0.40(6)	1.03(11)	0.080(1)	1.9836(4)	2.548(4) 2.683(1) 2.406(1)	2.2326(5)	5.60	6.78	1.76
$Bi_{1.750}Yb_{0.250}Ru_2O_7$	0.2399(4)	0.3278(1)	0.73(5)	0.96(11)	0.045(1)	1.9838(4)	2.539(4) 2.661(1) 2.411(1)	2.2286(4)	5.40	6.65	1.80
$Bi_{1.625}Yb_{0.375}Ru_2O_7$	0.2403(5)	0.3284(1)	0.74(6)	0.86(15)	0.046(1)	1.9839(5)	2.532(5) 2.649(1) 2.409(1)	2.2258(6)	6.07	7.61	1.73
$Bi_{1.500}Yb_{0.500}Ru_2O_7$	0.2404(5)	0.3290(2)	0.62(7)	0.82(19)	0.030(1)	1.9844(7)	2.524(6) 2.640(2) 2.403(2)	2.2231(6)	5.66	6.70	1.60
$Bi_{1.375}Yb_{0.625}Ru_2O_7$	0.2410(6)	0.3298(2)	0.65(7)	0.77(231)	0.043(1)	1.9853(7)	2.516(6) 2.624(2) 2.402(2)	2.2201(7)	5.51	6.55	1.57
$Bi_{1.250}Yb_{0.750}Ru_2O_7$	0.2413(6)	0.3303(2)	0.66(7)	0.68(24)	0.034(1)	1.9854(7)	2.509(7) 2.614(2) 2.399(2)	2.2176(8)	5.88	7.03	1.66
$Bi_{1.125}Yb_{0.875}Ru_2O_7$	0.2424(6)	0.3311(1)	0.70(6)	0.73(19)	0.004(1)	1.9862(5)	2.499(7) 2.591(2) 2.404(2)	2.2137(7)	6.31	7.70	1.77
$Bi_{1.000}Yb_{1.000}Ru_2O_7$	0.2423(7)	0.3318(2)	0.61(7)	0.77(20)	0	1.9859(5)	2.491(7) 2.584(2) 2.394(2)	2.2103(8)	6.59	8.01	1.82
$Bi_{0.875}Yb_{1.125}Ru_2O_7$	0.2421(4)	0.3325(1)	0.41(5)	0.57(18)	0	1.9861(5)	2.482(5) 2.577(1) 2.384(1)	2.2071(5)	5.23	6.47	1.63
$Bi_{0.750}Yb_{1.250}Ru_2O_7$	0.2433(5)	0.3333(1)	0.42(4)	0.62(15)	0	1.9850(5)	2.470(5) 2.550(1) 2.387(1)	2.2013(6)	5.06	6.27	1.61
$Bi_{0.625}Yb_{1.375}Ru_2O_7$	0.2439(6)	0.3343(1)	0.42(4)	0.67(15)	0	1.9859(5)	2.459(6) 2.532(1) 2.383(1)	2.1972(7)	4.74	5.82	1.49

[a] The atoms are at the following positions in space group $Fd3m$ (No. 227) Bi onto a 96h ($^1/_2$, $^1/_2 + y$, $^1/_2 - y$), Ru 16c (0, 0, 0), O(1) 48f (x, $^1/_8$, $^1/_8$), and O(2) 8b (0.375, 0.375, 0.375).

boring oxygen atoms. Attempts to verify this by allowing the O′ atom to be disordered at a 32e site (x, x, x), $x \approx 0.375$, were inconclusive.

We find that the magnitude of the displacement of the A-type cation reduces as the Yb content increases (Table 4). Attempts to model either the synchrotron or neutron diffraction data in which the Bi was displaced onto the 96h site while the Yb remained on the 16d site were inconclusive. It is not possible to ascertain whether both types of cations were equally displaced. We note that inclusion of the Bi cation displacement in the structural model did not change either the value of the variable oxygen position parameter nor did it alter the magnitude of the displacement of the Ru and O atoms. It did, however, result in a small but apparently significant decrease in the 16d displacement parameters for the O′ atoms suggesting these are actually on the 32e site. Equally, it decreased the effective bond valence sums for these cations (Table 3).

Figure 5 demonstrates that the replacement of the bismuth by ytterbium in $Bi_{2-y}Yb_yRu_2O_{7-\delta}$ results in a systematic decrease in the lattice parameter. Presumably this is a consequence of smaller size of ytterbium (0.985 Å) relative to bismuth (1.17 Å). However, a linear fit to these data was relatively poor and the plot could be divided into two sections, that for compositions below $y \approx 0.9$ and those above. The single variable positional parameter, x, of the oxygen atoms on the 48f sites, also

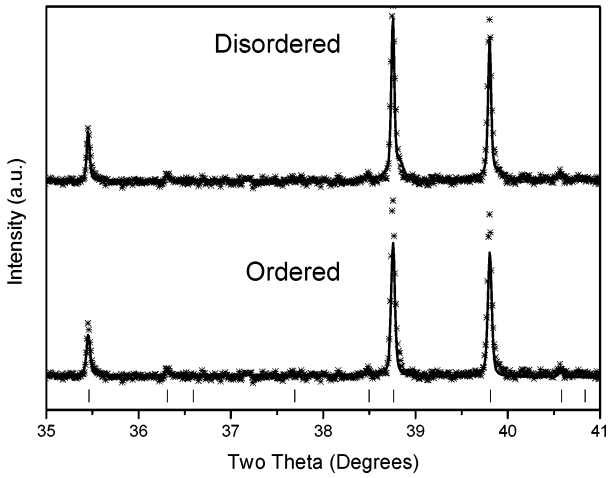

Figure 6. Portion of the observed and calculated synchrotron diffraction profiles for $Bi_{1.375}Yb_{0.625}Ru_2O_{7-\delta}$. The solid lines were calculated using the standard ordered pyrochlore model and with the Bi atoms disordered onto the 96h sites ($\lambda = 0.782$ Å).

Table 5. Calculated Bandwidth for the Two Series $Bi_{2-y}Yb_yRu_2O_{7-\delta}$ and $Bi_{2-y}Nd_yRu_2O_{7-\delta}$[a]

$Bi_{2-y}Yb_yRu_2O_7$	t_{2g} bandwidth (eV)	$Bi_{2-y}Nd_yRu_2O_7$	t_{2g} bandwidth (eV)
0	1.051	0	1.051
0.125	1.039	0.25	1.04
0.25	1.032	0.5	1.024
0.375	1.025	0.75	1.02
0.5	1.022	0.825	0.9984
0.625	1.008	0.925	0.9956
0.75	1.005	1	1.0147
0.875	0.992	1.25	0.9835
1	0.985	1.5	0.9739
1.125	0.977	1.75	0.9563
1.25	0.972	2	0.9406
1.375	0.958		
2	0.91		

[a] The structural parameters for the Nd compounds were taken from ref 13.

shows a systematic increase with increasing Yb content, but again a simple linear fit was unsatisfactory and a change of slope was apparent near $y \approx 0.9$, Figure 5. The substitution of Yb ions for Bi ions leads to the distortion of RuO_6 octahedra, elongation of the Ru−O bond lengths, and the reduction of Ru−O−Ru angles. The distortion of RuO_6 octahedron can also be described by the changes of the O−Ru−O angles. There are two types of unequal O−Ru−O angles in the Ru_2O_6 sublattice. As the Yb content increases, the first of these increases from 95.34°(4) in $Bi_2Ru_2O_{7-\delta}$ to 99.34°(4) in $Yb_2Ru_2O_7$ and the second decreases from 84.67°(4) to 80.66°(5). Both the short and long Bi(Yb)−O bond lengths decrease with increasing Yb content across the entire series, presumably as a consequence of the smaller size of the Yb^{3+} cations. The Ru−O bond distance shows a general increase as the Yb content is increased; although this is clearly not linear, as there is an apparent change in gradient near $y = 1$. The Ru−O−Ru angles show a linear reduction with increasing Yb content from 133.33°(5) in $Bi_2Ru_2O_{7-\delta}$ to 127.18°(7) in $Yb_2Ru_2O_7$ (Figure 5).

At this stage it is appropriate to compare the present structural results with those for $Bi_{2-y}Nd_yRu_2O_{7-\delta}$ described by Field et al.[13] The estimated standard deviations of the structural parameters reported by Field are approximately the same as those reported here. In both $Bi_{2-y}Nd_yRu_2O_{7-\delta}$ and $Bi_{2-y}Yb_yRu_2O_{7-\delta}$, the vacancies on the O′ site exist over the Bi-rich range $0.0 \le y \le 0.75$, whereas this site is fully occupied over the Bi-poor range $0.75 < y \le 2.0$. Second, with increasing lanthanide content, the lattice parameters increase in $Bi_{2-y}Nd_yRu_2O_{7-\delta}$ whereas they decrease in $Bi_{2-y}Yb_yRu_2O_{7-\delta}$. The decrease of the lattice parameters in $Bi_{2-y}Yb_yRu_2O_{7-\delta}$ with increasing Yb content is readily explained by the difference in the size of the Yb^{3+} (0.985 Å) and Bi^{3+} (1.17 Å) cations. The ionic radius for Nd^{3+} (1.109 Å) is marginally smaller than that for Bi, yet the lattice parameter $Bi_{2-y}Nd_yRu_2O_{7-\delta}$ increases with increasing Nd content apparently as a consequence of the sterochemical effect of the Bi 6s lone pair.[13,40] Finally, the general composition dependence of the refined oxygen positional parameter is similar in the two series: in both cases it increases as the rare earth content is increased. Whereas Field et al.[13] noted a noticeable discontinuity at the metal−semiconductor transition point near $y = 1$ we observe a much more subtle transition near $y = 0.9$ in the Yb series. Clearly there are subtle structural changes across the series and identifying these is not always straightforward.

A geometrical argument, first presented by Whangbo, can be used to explain the observed changes in the electronic properties of the ruthenium pyrochlores.[24] Replacement of the Yb by a larger Bi cation will result in movement of the oxygen atoms away from the Bi cation (along the bisector of the Ru−O−Ru angle), thereby increasing the Ru−O−Ru angle and shortening the Ru−O bond length, Figure 7. However, unlike the almost linear change in the Ru−O−Ru angle, there is a discontinuous variation in the Ru−O bond distance near $y = 0.75$ that is at about transition to the metallic state. As stated above the Ru−O bond distance is dependent on both the O′ position and lattice parameter. Field et al.[13] suggested that the presence of oxygen vacancies is likely to be important for the metallic behavior in ruthenium pyrochlores. One effect of oxygen vacancies is that it allows the lattice parameters to contract resulting in a shortening of the Ru−O bond lengths, and it is observed that the largest reduction in the Ru−O bond lengths occurs in those oxides that also have oxygen vacancies. An additional factor that may influence Ru−O bond distance is the bonding within the $AO_6O'_2$ scalehedron. The Bi bond valence is dominated by the short Bi−O bond, hence a change in the Bi-(Yb)−O bonding is likely to influence the structure of pyrochlore oxides. Such changes are possible as a result of the participation of the $6s^2$ lone pair of Bi^{3+} in the bonding. The sterochemical activity of these electrons in a BiO_8 environment is well-documented[40] and acts to increase the effective size of the ion, provided there is no long range ordering of their displacement.

Electronic Band Structure. The Ru 4d t_{2g} bandwidths for the two series of oxides $Bi_{2-y}Yb_yRu_2O_7$ and $Bi_{2-y}Nd_yRu_2O$ were calculated using the program Caesar.[37] The results are illustrated in Figure 8. For both series the replacement of the polarizable bismuth atoms with a lanthanide atom results in a decrease of the t_{2g} bandwidth. Although there is some scatter in the calculated bandwidths it is immediately apparent from Figure 8 that the bandwidths of the Yb series are

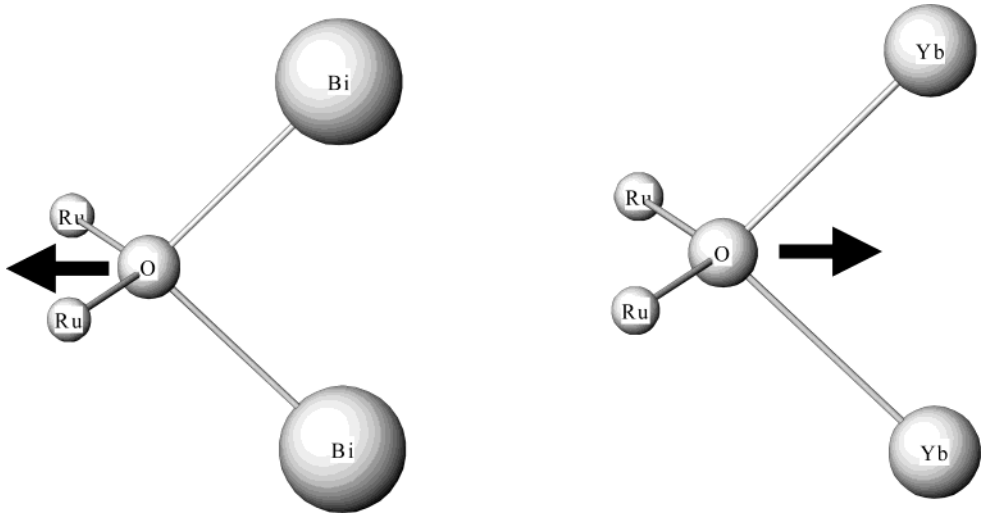

Figure 7. Coordination environment of the O atoms in the ruthenium pyrochlores illustrating the effect of the size of the A-type cation on the environment of the Ru atoms. The large Bi atoms increases the Ru−O−Ru bond angle and shortens the Ru−O bond, whereas the smaller Yb cation decreases the Ru−O−Ru bond angle and lengthens the Ru−O bond.

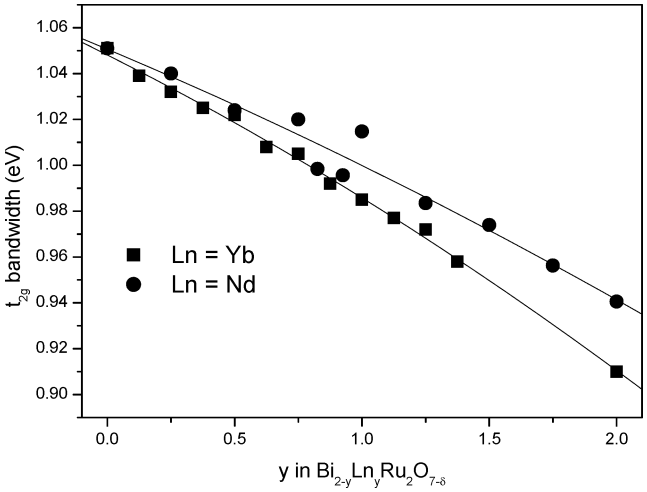

Figure 8. Composition dependence of the width of the t_{2g} band in the two series $Bi_{2-y}Ln_yRu_2O_{7-\delta}$.

systematically smaller than those for the Nd series in the semiconducting oxides. This is a consequence of the relative size of the Yb and Nd cations. Despite this difference in size the calculated bandwidths for the two series become approximately equal near $y \approx 1$, that is the point at which metallic conductivity is observed.

Conclusions

Precise structures have been refined for 13 members in the series $Bi_{2-y}Yb_yRu_2O_{7-\delta}$ using high-resolution powder neutron diffraction methods. Variable-temperature resistivity studies have confirmed that a transition from metallic to semiconducting behavior is observed as the Yb content is increased and this occurs when $y \approx 0.9$. This critical point does not correspond to any dramatic changes in either the unit cell size or the key Ru−O−Ru bond angles. It does, however, represent the point at which appreciable oxygen vacancies are observed in the Bi rich metallic oxides, and these are observed to have slightly smaller Ru−O bond lengths than those for the semiconducting oxides.

Band structure calculations show the width of the Ru t_{2g} band is systematically smaller in the series $Bi_{2-y}Yb_yRu_2O_{7-\delta}$ than in $Bi_{2-y}Nd_yRu_2O_{7-\delta}$ as a consequence of the smaller size of Yb^{3+} relative to Nd^{3+} or Bi^{3+}. There is a smooth progression in the bandwidth as the Yb content is altered, and as expected from the structural parameters it is not possible to identify a clear break between the metallic and semiconducting oxides.

An unexpected observation in this work is the presence of static disorder of the Bi cations in the Bi rich compounds. This disorder was confirmed by synchrotron X-ray diffraction measurements and appears to be related to the sterochemical activity of the Bi 6s electrons. The displacement of the Bi from ($^1/_2$, $^1/_2$, $^1/_2$) to a nearby 96h site at ($^1/_2$, $^1/_2 + y$, $^1/_2 - y$) acts to overcome the under bonding of the Bi in the ruthenium pyrochlores. Further studies, involving variable-temperature diffraction measurements, of this disorder are in progress.

Acknowledgment. This work was partially supported by the Australian Research Council. We thank the Australian Institute of Nuclear Science and Engineering for access for the neutron diffraction measurements and Dr. B. A. Hunter (ANSTO) for collecting the data. This work performed at the Australian National Beamline Facility was supported by the Australian Synchrotron Research Program, which is funded by the Commonwealth of Australia under the Major National Research Facilities program. Professor K. S. Murray and Dr. B. Moubaraki (Monash University) are thanked for their assistance with the conductivity measurements.

CM034503Q